Embedding PMU Algorithms in Grid-Following Converters: a Feasibility Study

Atul Singh, David Macii, Dario Petri

Dep. of Industrial Engineering, University of Trento, Trento, Italy, 38123
E-mail: atul.singh@unitn.it, david.macii@unitn.it, dario.petri@unitn.it

Abstract

One of the most critical challenges in the evolution of smart grids is the shortage of measurement devices at the distribution level, coupled with the high costs associated with extensive refurbishment of the existing monitoring infrastructure. To address this issue, this paper investigates the feasibility of upgrading the controllers of smart Power Electronic Converters (PECs) to turn them into auxiliary measurement devices, thereby improving system observability. Specifically, an algorithm originally conceived for a Phasor Measurement Unit (PMU) is adapted to meet both the Class P specifications of the IEEE Standard IEC/IEEE 60255-118-1:2018 and the requirements for grid connection reported in the IEEE Standard 1547-2023. Several simulation results confirm the validity of the general idea, although some concerns remain on the algorithm computational burden to ensure real-time performance.

Keywords

Phasor Measurement Units (PMU), Grid-Following Converters, Distribution Systems, Distributed Energy Resource (DER) interconnection.

I. Introduction

Achieving accurate, real-time state estimations that can effectively support power flow control actions under dynamic power demand and supply conditions is a well-recognized challenge in active smart grids [1]. One of the main problems lies in the economic and infrastructural constraints that limits the wide-scale deployment of high-accuracy measurement devices, such as the Phasor Measurement Units (PMUs) [2], [3]. The need for advanced power flow control techniques is expected to grow further with the proliferation of electric vehicles and renewable energy communities [4], wherein the exploitation of Distributed Energy Resources (DERs) must be optimized without jeopardizing grid stability [5], [6]. The limited distribution systems observability due to the shortage of measurement points can be easily addressed using virtual measurements (e.g., zero power injections at buses without loads) or pseudo-measurements (e.g., based on aggregated historical active and reactive power data) [7]. However, this approach comes at the cost of reduced state estimation accuracy, particularly under highly dynamic operating conditions [8].

To improve state estimation capability and performance, two complementary approaches exist. The most obvious one is to place high-rate, high-accuracy synchronized instruments like the PMUs in strategic points of the distribution system to maximize observability, while minimizing deployment costs [9]–[12].

Alternatively, the grid measurement and monitoring capabilities can be enhanced by leveraging or upgrading existing devices, most notably those of the Advanced Metering Infrastructure (AMI) [13]–[16]. In fact, the different rate and lack of synchronization of different measurement data, although critical for performance, can be kept under control [17].

An emerging approach, that somehow extends the previous one, concerns with upgrading other existing devices to insert additional measurement points into the grid, thereby improving system observability. An interesting example of this idea is reported in [18], where the data collected from both smart inverters of photovoltaic (PV) generators and weather stations are merged with the measurement data typically used for distribution system state estimation. In particular, the idea of using the smart controllers of power converters as auxiliary measurement devices is rather innovative and, in our opinion, it deserves to be investigated in depth for the following reasons.

- The grid-forming and grid-following Power Electronic Converters (PECs) are essential for grid integration of DERs. Also, their number is expected to grow as a result of the increasing penetration of renewable energy sources and energy communities [6]. As a result, if the PECs could measure one or more electrical quantities, especially at the point of common coupling (PCC), system observability could be significantly enhanced with minimal additional costs.

This work was funded by the European Union - Next Generation EU, Mission 4, Component 2, through the Italian Ministerial grant PRIN 2022 "Smart grid-connected power converters based on advanced synchrophasor-inspired harmonics measurements for holistic integration of renewable energy sources (POWERHERO)," n. 20224X2AYH, CUP F53D23000490006.

- Smart PECs already perform several ancillary functions such as, for instance, volt/var optimization, active power flow management, and last but not least, power quality monitoring and control. For this reason, the Root Mean Square (RMS) amplitude of ac voltage and current waveforms, voltage frequency on the Electric Power System (EPS) side, as well as active and reactive power and Total Harmonic Distortion (THD) are already measured locally and a low rate to support the connection of DERs to the EPS.
- DER interconnection and interoperability must meet tight grid synchronization requirements that are typically achieved through ad-hoc Phase Lock Loops (PLLs). Interestingly, some PMU prototypes also adopt a PLL-based architecture [19], [20]. This similarity suggests that synchrophasor measurement and DER connection functions may share common features. However, a critical distinction between them is that no Coordinated Universal Time (UTC) reference is needed to connect a DER to the grid. Therefore, a UTC-based time reference should be connected to the PEC controller. To this end, the Precision Time Protocol (PTP), and particularly, the IEEE C37.238-2017 standard PTP profile for power system applications could be used [21], [22].
- Finally, it is important to note that smart PECs should not be considered standalone devices. In the future, they are expected to communicate and cooperate to enhance grid resilience and stability [23]. Therefore, these devices will likely be equipped with networking capabilities, which could also be used to gather and share measurement data.

Based on the general remarks listed above, the objective of this paper is to investigate the feasibility of using the same algorithm within a given PEC controller both as a P Class PMU (i.e., for protection purposes) and for DER connection. In fact, this is the first step to transform the PEC controller into an additional measurement device for distribution system monitoring.

To the best of Authors' knowledge, only another research prototype was developed in the recent past for the same purpose [24]. However, it utilized a basic Discrete Fourier Transform (DFT) for synchrophasor estimation and offered limited control functions. Therefore, the potential of either integrating PMU-like algorithms for DER connection into PEC controllers or, vice versa, upgrading the existing PLL inside PECs to transform them into embedded PMUs, is still vastly unexplored. For this reason, this paper presents a preliminary study on the feasibility of this general idea. First, in Section II, a synchrophasor estimation algorithm based on the combination of the solution presented in [25] and [26] is briefly described. Then, in Section III the same algorithm is characterized in a variety of testing conditions to find the best settings for both synchrophasor measurement (i.e., in compliance with the P Class requirements of the IEC/IEEE Standard 60255-118-1:2018 [27]), and DER connection purposes (e.g., following the requirements of the IEEE Standard 1547-2023 [28]). Finally, Section IV concludes the paper and outlines the future work.

II. Algorithm description

As known, the PMUs are designed to measure amplitude, phase angle, frequency, and rate of change of frequency (ROCOF) of fundamental AC voltage or current waveforms at instants synchronized to the UTC. The algorithm adopted in this paper relies on the dynamic phasor model originally described in [29] and further extended in [30] for harmonics estimation though the so-called Taylor-Fourier Transform (TFT).

A voltage or current signal including H harmonics and observed in an interval of duration $T = \frac{N}{f_s}$ (where N is an integer odd number and f_s is the sampling frequency) can be modeled as:

$$s\left(t\right) = \sum_{h=1}^{H} a_h\left(t\right) \cos\left(2\pi f_h t + \theta_h(t)\right), \quad -\frac{T}{2} \leq t \leq \frac{T}{2} \tag{1}$$

where $a_h\left(t\right)$, f_h and $\theta_h(t)$ are the amplitude, the frequency and the phase of the $h-$th harmonic component, respectively, at time t. Note that in (1) magnitude and phase of all phasors are assumed to be time-varying quantities, whereas the harmonic frequencies are regarded as stationary. If the phasor of each harmonic within a given observation interval is described by its Taylor's series centered at time $t_c = \frac{n}{f_s}$ and truncated to order K_h (for $h = 1, \ldots, H$) the discrete-time signal model (1) can be rewritten as

$$\begin{aligned} s\left(t\right) =& \sum_{h=1}^{H} \frac{1}{2}\left[p_h\left(t\right) e^{j2\pi f_h t} + \overline{p}_h\left(t\right) e^{-j2\pi f_h t}\right] \approx \\ \approx& \frac{1}{2} \sum_{h=1}^{H} \left[\left(\sum_{k=0}^{K_h} \frac{p_{h,k}(n)}{f_s^k k!} \ell^k \right) e^{j2\pi \frac{f_h}{f_s}(n+\ell)} + \right. \\ & \left. \left(\sum_{k=0}^{K_h} \frac{\overline{p}_{h,k}(n)}{f_s^k k!} \ell^k \right) e^{-j2\pi \frac{f_h}{f_s}(n+\ell)} \right] - \frac{N-1}{2} \leq \ell \leq \frac{N-1}{2} \end{aligned} \tag{2}$$

where $p_h\left(t\right) = a_h\left(t\right) e^{j\theta_h(t)}$ and $\overline{p}_h\left(t\right) = a_h\left(t\right) e^{-j\theta_h(t)}$ is the pair of complex conjugate dynamic phasors of the $h-$th harmonic, while $p_{h,k}(n)$ and $\overline{p}_{h,k}(n)$ are the $k-$th order derivatives of the same pair of complex conjugate dynamic phasors computed in the center of the considered observation interval, i.e., at time t_c.

If the signal samples of (2) are arranged into the column vector $\mathbf{s}_n = \left[s\left(\frac{n-N/2}{f_s}\right), \ldots s\left(\frac{n+N/2}{f_s}\right)\right]^T$ and the Taylor's series coefficients of all harmonics are gathered into vector $\mathbf{p}_n = \left[p_{1,0}(n), \overline{p}_{1,0}(n), \ldots, p_{H,K_H}(n), \overline{p}_{H,K_H}(n)\right]^T$, then (2) can be more compactly expressed in a matrix form as explained in [26], [31], i.e.,

$$\mathbf{s}_n = \mathbf{G}(\mathbf{f})\mathbf{p}_n \tag{3}$$

where the system matrix $\mathbf{G}(\cdot)$ includes orderly all the pairs of terms $\frac{\ell^k}{f_s^k k!}e^{j2\pi\frac{f_h}{f_s}(n+\ell)}$ and $\frac{\ell^k}{f_s^k k!}e^{-j2\pi\frac{f_h}{f_s}(n+\ell)}$ for $-\frac{N-1}{2} \leq \ell \leq \frac{N-1}{2}$ and $\mathbf{f} = [f_1, \ldots, f_H]^T$ is the vector including all the harmonic frequencies. Since (3) is a linear system, in principle the coefficients of all harmonic phasors could be easily estimated by inverting the system, i.e.,

$$\widehat{\mathbf{p}}_n = \left(\mathbf{G}^H(\mathbf{f})\mathbf{G}(\mathbf{f})\right)^{-1}\mathbf{G}^H(\mathbf{f})\mathbf{s}_n \tag{4}$$

where ^{H} denotes the Hermitian operator. However, several issues arise, i.e.,

- The estimator algorithm accuracy can be greatly improved if the samples in $\mathbf{s}_n$ are weighted by a window function smoothing the Taylor's series errors at the end of each observation interval [26], [30].
- the elements of $\mathbf{f}$ are just approximately known a priori due to the presence of possible off-nominal frequency deviations.
- The computational complexity of the overall estimator for a given number of samples N tends to grow cubically with the number $K_{tot} = \sum_{h=1}^{H} K_h$ of harmonics' Taylor's series coefficients included in the model. This is due to the fact that the size of matrix $\mathbf{G}^H(\mathbf{f})\mathbf{G}(\mathbf{f})$ in (4) is $2K_{tot} \times 2K_{tot}$ and the computational complexity of matrix inversion is about $O(K_{tot}^3)$.

To address the first problem a tunable Kaiser window was used in this paper as in [26], i.e.,

$$w(\ell) = \frac{I_0\left(\beta\sqrt{1-\left(\frac{2\ell}{N-1}-1\right)^2}\right)}{I_0(\beta)}, \; -\frac{N-1}{2} \leq \ell \leq \frac{N-1}{2} \tag{5}$$

where $I_0(\cdot)$ is the 0-order modified Bessel function of the first kind, and β is a parameter that allows for a trade-off between the width of the spectral main-lobe and the magnitude of the spectral side-lobes. Specifically, a larger β value lowers the side-lobe level at the cost of wider main-lobe and vice versa. For this reason, the algorithm sensitivity to β variations shall be analyzed in this work.

The issue of excessive computational burden can be mitigated by applying the results of the analysis presented in [25]. Indeed, it is shown in that work that the impact of harmonics depends on the observation interval length. If the observation interval is kept as short as possible, (i.e., 2 nominal cycles) to achieve the best performance in terms of accuracy, responsiveness and speed, just the first four harmonics [25] should be included in the model. Moreover, unlike the fundamental component (whose dynamic fluctuations are significant over time), the first- and second-order derivatives of the harmonics phasors do not impact on accuracy significantly. Therefore, in (2)-(4), we can set $H = 4$ and $K_1 = 2$, $K_2 = K_3 = K_4 = 0$.

Finally, to reduce the uncertainty due to possible off-nominal deviations, the adopted TFT approach is applied twice, i.e., first assuming that both fundamental and harmonics take their respective nominal values, and then using the frequency estimates resulting from this stage to refine the measurement of fundamental synchrophasor, fundamental frequency and ROCOF. The idea of estimating off-nominal frequency deviations in the preliminary stage is not new, as in the past both the Interpolated Discrete Time Fourier Transform (IpDFT) and a zero-crossing detection method were used in [25] and in [26], respectively. However, employing a double TFT stage of reduced complexity, as proposed, mitigates the impact of possible harmonics.

Entering into details, if the Kaiser window (5) is used to transform (4) into a weighted least-squares estimator, the first stage of the algorithm is based on the solution of the following system, i.e.,

$$\widehat{\mathbf{p}}_n^{(1)} = \left(\mathbf{G}^H(\mathbf{f}_0)\mathbf{W}^H\mathbf{W}\mathbf{G}(\mathbf{f}_0)\right)^{-1}\mathbf{G}^H(\mathbf{f}_0)\mathbf{W}^H\mathbf{W}\mathbf{s}_n \tag{6}$$

where $\mathbf{W} = \text{diag}\left(w(\frac{-N+1}{2}, \ldots, w(\frac{N-1}{2})\right)$ and $\mathbf{f}_0 = [f_0, \ldots, Hf_0]$, with f_0 being the nominal power system frequency (i.e., 50 Hz or 60 Hz). The zero- and first-order terms of the Taylor series of the fundamental synchrophasor extracted from $\widehat{\mathbf{p}}_n^{(1)}$ can then be used to estimate the frequency of the H harmonics (4 in this case) included in the model, i.e., [30]

$$\widehat{f}_h^{(1)} = h\left(f_0 + \frac{1}{2\pi}\frac{\text{Im}\left\{\widehat{p}_{1,1}^{(1)}\widehat{\overline{p}}_{1,0}^{(1)}\right\}}{\left|\widehat{p}_{1,0}^{(1)}\right|^2}\right), \;\; h = 1, \ldots, H \tag{7}$$

TABLE I
MAXIMUM RESPONSE TIMES AND OVERSHOOTS OF SYNCHROPHASOR, FREQUENCY, AND ROCOF ESTIMATES AFTER THE INPUT STEP CHANGES SPECIFIED IN IEC/IEEE STD. 60255-118-1:2018 [27].

Transient test	β	**Synchrophasor response time (cycles)**	**IEC/IEEE Std. Limit (cycles)**	**Frequency response time (cycles)**	**IEC/IEEE Std. Limit (cycles)**	**ROCOF response time (cycles)**	**IEC/IEEE Std. Limit (cycles)**	**Overshoot (%)**	**IEC/IEEE Std. Limit (%)**
$\pm 10\%$ Magnitude Step	2	0.45	2	1.02	4	1.02	6	0.80	5
	4	0.42	2	1.01	4	1.02	6	0.70	5
	6	0.39	2	0.98	4	1.02	6	0.60	5
$\pm 10^{\circ}$ Phase Step	2	0.93	2	1.02	4	1.02	6	0.15	5
	4	0.88	2	1.02	4	1.02	6	0.16	5
	6	0.79	2	1.02	4	1.02	6	0.17	5

Afterwards, the values returned by (7) and gathered into vector $\widehat{\mathbf{f}}^{(1)} = \left[\widehat{f}_1^{(1)}, \ldots, \widehat{f}_H^{(1)}\right]^T$ can be replaced into the system matrix $\mathbf{G}(\cdot)$ to refine the estimation of all the parameters of (1). Specifically, the second stage of the algorithm relies on the solution of a system similar to (6), i.e.,

$$\widehat{\mathbf{p}}_n^{(2)} = \left(\mathbf{G}^H(\widehat{\mathbf{f}}^{(1)})\mathbf{W}^H\mathbf{W}\mathbf{G}(\widehat{\mathbf{f}}^{(1)})\right)^{-1}\mathbf{G}^H(\widehat{\mathbf{f}}^{(1)})\mathbf{W}^H\mathbf{W}\mathbf{s}_n \tag{8}$$

Finally, the amplitude, phase, refined frequency and ROCOF of the fundamental component of (1) are extracted from the first entry of the vector (8) as follows [30]:

$$\widehat{a}_1 = 2\left|\widehat{p}_{1,0}^{(2)}\right|,\ \widehat{\theta}_1 = \arg\left\{\widehat{p}_{1,0}^{(2)}\right\} \tag{9}$$

$$\widehat{f}_1 = \widehat{f}_1^{(1)} + \frac{1}{2\pi}\frac{\mathrm{Im}\left\{\widehat{p}_{1,1}^{(2)}\widehat{\widehat{p}}_{1,0}^{(2)}\right\}}{\left|\widehat{p}_{1,0}^{(2)}\right|^2} \tag{10}$$

$$\widehat{R}_1 = \frac{1}{\pi}\left[\frac{\mathrm{Im}\left\{\widehat{p}_{1,2}^{(2)}\widehat{\widehat{p}}_{1,0}^{(2)}\right\}}{2\left|\widehat{p}_{1,0}^{(2)}\right|^2} - \frac{\mathrm{Re}\left\{\widehat{p}_{1,1}^{(2)}\widehat{\widehat{p}}_{1,0}^{(2)}\right\}\mathrm{Im}\left\{\widehat{p}_{1,1}^{(2)}\widehat{\widehat{p}}_{1,0}^{(2)}\right\}}{\left|\widehat{p}_{1,0}^{(2)}\right|^4}\right] \tag{11}$$

While expressions (9)-(11) could be used to update the quantities of interest any time a new waveform sample is collected, frequency and ROCOF estimates can be averaged over one fundamental cycle to reduce the impact of wideband noise.

III. SIMULATION RESULTS

A. PMU compliance tests

In this Section, the performance of the algorithm described in Section II is first analyzed under the Class P testing conditions reported in the IEC/IEEE Standard 60255-118-1:2018 [27], assuming that the sampling rate is $f_s = 6$ kHz (that is, $M = 120$ or $M = 100$ samples are collected in a single nominal voltage cycle at 50 Hz or 60 Hz, respectively) and observation intervals of $C = 2$ fundamental periods. In addition, in all tests an additive noise floor corresponding to a Signal-to-Noise Ratio (SNR) of 80 dB was considered. Such noise (although not mentioned in [27] does not include the wide-band disturbances injected from the EPS through the voltage/current measurement transducers, but it keeps into account the noise affecting the signal acquisition front-end of a high-resolution measurement device. The bar diagrams of the maximum values of Total Vector Errors (TVE), Frequency Estimation Errors (FE) and ROCOF Estimation Errors (RFE) computed over observation intervals shifted by one sample at a time for a total duration of about 2 seconds are shown in Fig. 1(a)-(c), respectively. The triples of bars within each group refer to alternative Kaiser windows (i.e., assuming that parameter $\beta = \{2, 4, 6\}$ and refer to the following P Class testing conditions, i.e.

- **Off-nominal Deviation (OD)**: the RMS value of the fundamental component linearly changes from 0.8 p.u. to 1.2 p.u. at 0.1 p.u. steps and the system frequency linearly changes by ± 2 Hz at 0.1 Hz steps.
- **Harmonic Distortion (HD)**: all the harmonics from the 2nd to the 50th are added (one at a time) to the fundamental term. The RMS value of each added harmonic is 1% of the fundamental.
- **Amplitude Modulation (AM)**: the voltage amplitude is affected by 10% sinusoidal amplitude modulation with a modulating tone frequency of 2 Hz.
- **Phase Modulation (PM)**: the voltage amplitude is affected by a sinusoidal phase modulating tone of amplitude 0.1 rad and frequency 2 Hz.
- **Frequency Ramp (FR)**: the signal frequency is increased or decreased linearly by no more than ± 2 Hz with respect to the fundamental frequency at a rate of ± 1 Hz/s.

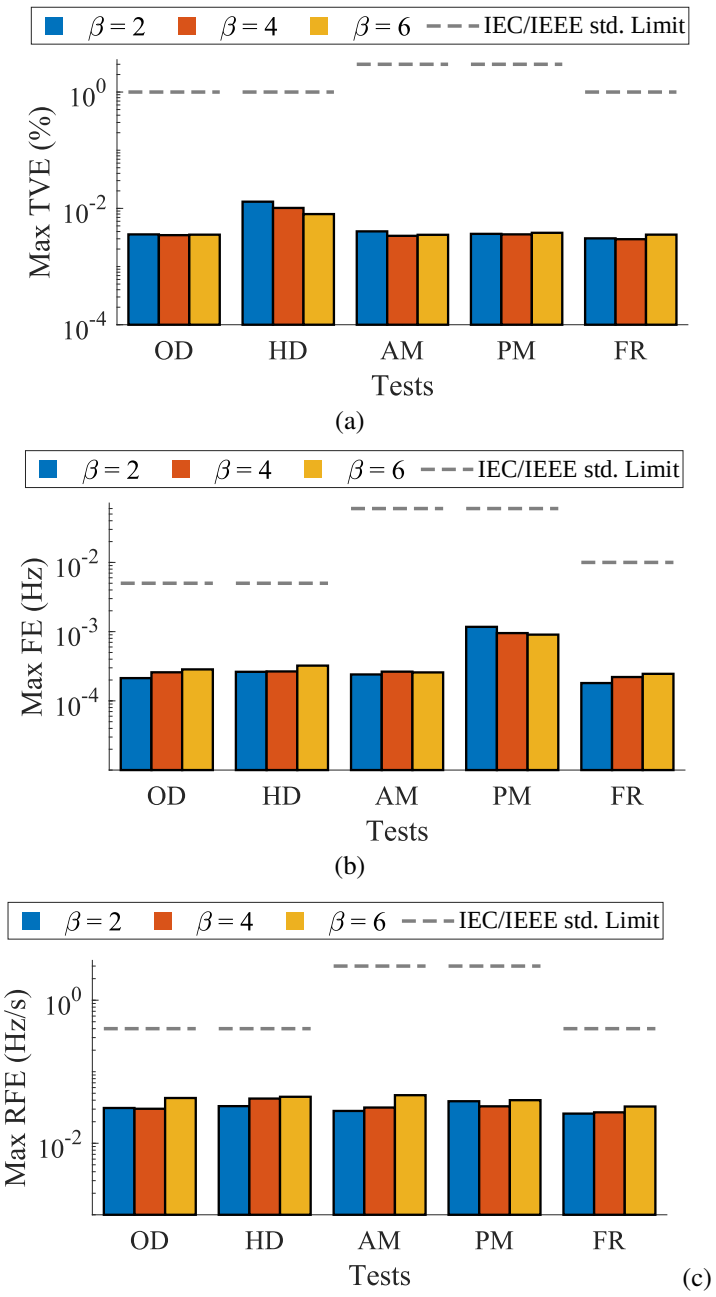

Fig. 1. Maximum (a) TVE, (b) FE and (c) RFE values in different P Class testing conditions reported in the IEC/IEEE Standard 60255-118-1:2018 [27]. Different bars refer to different values of the β parameter of the Kaiser window, while the dashed lines represent the IEC/IEEE Standard limits in various testing conditions.

The dashed lines in Fig. 1(a)-(c) represent the P Class limits specified in the IEC/IEEE Standard 60255-118-1:2018 in the various testing conditions listed above [27].

Clearly, the P Class limits are safely met in all cases and for any value of β. Interestingly, simulations showed that the inclusion of the 2nd, 3rd and 4th harmonic phasors in the vector of parameters to be estimated makes their impact on fundamental synchrophasor, frequency and ROCOF measurement almost negligible, with results that are comparable with those obtained with off-nominal frequency and amplitude deviations only. Moreover, the increasing equivalent noise bandwidth of the Kaiser window for larger values of β has a minor impact on results if SNR = 80 dB. Further results (omitted for the sake of brevity) show that in the OD case, this performance gap tends to grow, especially as far as the FE and RFE values are concerned. This means that it is reasonable to keep the value of β moderate. In fact, setting $\beta > 4$ just increases the sensitivity to wideband noise with no significant benefits in terms of harmonic rejection or synchrophasor tracking capability. The estimation errors in

TABLE II
COMPARISON BETWEEN THE MAXIMUM VOLTAGE MAGNITUDE, PHASE, AND FREQUENCY DIFFERENCES SPECIFIED IN [28], AND THE MEASUREMENT ACCURACY ACHIEVED BY THE PROPOSED ALGORITHM AT THE END OF THE INTERCONNECTION TRANSIENT.

	IEEE Std. 1547-2018 limits for DER-EPS interconnection			**Algorithm Accuracy**
	$\mathbf{P \leq 500}$ **kVA**	$\mathbf{500 < P \leq 1500}$**kVA**	$\mathbf{P > 1500}$ **kVA**	
$\mathbf{\Delta V}$ **(%)**	10	5	3	**0.32**
$\mathbf{\Delta f}$ **(mHz)**	300	200	100	**25.1**
$\mathbf{\Delta \Phi}$ **(°)**	20	15	10	**0.12**

dynamic testing conditions (i.e., in the AM, PM and FR cases) confirm a rather low sensitivity to the increments of β.

Table I reports the maximum response times of the synchrophasor, frequency and ROCOF estimates, respectively, after $\pm 10\%$ magnitude step or $\pm 10^{\circ}$ phase step changes, as specified in the IEC/IEEE Standard 60255-118-1:2018 [27]. Such times are expressed in nominal waveform cycles and compared with the IEC/IEEE Standard limits. The relative size of the magnitude overshoots after each kind of steps is also shown. The maxima are determined by linearly varying the step's occurrence instant across one fundamental cycle. The results of all tests reveal an excellent responsiveness of the considered algorithm, regardless of the value of the Kaiser window's β parameter. In conclusion. the algorithm is a good candidate to monitor the connection and disconnection of DERs, as well. A further interesting point is that the IEEE Standard 1547-2018 specifies voltage magnitude and frequency measurement accuracy limits within $\pm 1\%$ and ± 10 mHz in steady-state conditions and $\pm 2\%$ and ± 100 mHz during transients, respectively [28]. These limits are clearly more relaxed compared to those of the IEC/IEEE Standard 60255-118-1:2018, which requires compliance over 10 cycles under steady-state conditions and over 5 cycles under transient conditions. Therefore, the proposed algorithm can safely meet these requirements over 2-cycle intervals only, providing better accuracy and responsiveness.

B. DER connection/disconnection compliance tests

In this Section, the performance of the algorithm described in Section II for $\beta = 4$ is evaluated against selected grid code requirements outlined in the IEEE Standard 1547-2018 for DER connection and disconnection [28]. Table II compares: i) the maximum allowable RMS amplitude, frequency, and phase differences between voltage waveforms at the interface between the EPS and DER for different DER rated power levels; and ii) the measurement uncertainty range of the same quantities achieved by the proposed algorithm at the end of the transient for connecting a DER to the EPS. The maximum errors were determined through Monte Carlo simulations conducted under borderline yet realistic operating conditions. Specifically, the connection of a DER to a medium voltage EPS affected by a static frequency deviation within ± 3 Hz, a Total Harmonic Distortion (THD) equal to 8% (arising from the superimposition of the first 25 harmonics of varying magnitudes), and a Signal-to-Noise Ratio (SNR) of 55 dB at the point of DER connection. For each off-nominal frequency deviation, 120 simulation runs were performed using the same data acquisition settings described in III-A.

The results in Table II show that the algorithm accuracy in measuring the difference of pairs of voltage magnitude, frequency and phase at the point of DER connection is well below the most stringent limits reported in [28], even under rather noisy operating conditions of the grid. This confirms that the proposed algorithm could be potentially used to synchronize the interconnection of a DER to the EPS. While the settling time of the connection itself depends of course on the control loop within the PEC (which is out of the scope of this paper), it was verified that with the current simulation settings the maximum response times of the algorithm is in the order of about 1 cycle, that is orders of magnitude lower than the typical enter service periods specified in [28] (that are indeed in the order of seconds).

Further simulations were performed to test the ability of the proposed algorithm to detect timely the most severe abnormal conditions leading to DER tripping according to the IEEE Standard 1547-2018 [28]. In particular, four complementary different testing conditions were considered:

- a sudden voltage amplitude increase by 20%;
- a sudden voltage amplitude drop by 50%;
- a sudden voltage frequency increase by 2 Hz;
- a sudden voltage frequency decrease by -3 Hz.

In all the testing conditions listed above, the SNR of the EPS voltage signal is again 55 dB, while the THD is lower than in the DER connection scenario (i.e., 3%). Table III presents the maximum time taken by the algorithm to converge within $\pm 1\%$ of the magnitude estimates and within ± 10 mHz of the frequency changes after each step. These maxima are computed by randomly varying the time instant at which the step occurs within a given cycle. The results in Table III demonstrate

TABLE III
COMPARISON BETWEEN THE MAXIMUM SETTLING TIME OF THE MEASUREMENT ALGORITHM UNDER ABNORMAL MAGNITUDE AND FREQUENCY STEP CHANGES LEADING TO DER TRIPPING AND CLEARING TIME REQUIREMENTS OF THE IEEE STD. 1547-2018.

Testing condition	Variation	**Max. meas. settling time (s)**	**IEEE Std. 1547-2018 clearing time (s)**
Over-voltage step	$+20\%$	0.017	0.16
Under-voltage step	-50%	0.020	2.0
Over-frequency step	$+2$ Hz	0.020	0.16
Under-frequency step	-3 Hz	0.020	0.16

that the measurement settling times are one order of magnitude shorter than the maximum clearing times specified in [28]. Consequently, the proposed algorithm's timeliness is sufficiently rapid to support the required clearing operations.

C. Execution Time

The algorithm was implemented in MATLAB R2018b and tested on a laptop equipped with 16 GB RAM and an Intel Core i7-11370H processor running at 3.30 GHz. Execution times, under the settings described in Section III.A, ranged from approximately 4 ms to 7 ms, with an average of about 5.5 ms. This performance meets the reporting rate requirements specified in IEC/IEEE Standard 60255-118-1:2018 [27]. However, achieving sub-kilohertz update rates, which is crucial for grid-following converters control, requires further optimization. This could involve reducing the sampling rate and re-implementing the algorithm in C or C++, which has been shown to offer significant speed improvements over MATLAB, particularly for large-scale systems.

IV. CONCLUSION

This study has demonstrated the potential of embedding a synchrophasor estimation algorithm into a smart power electronic converter, to enable DER connection or disconnection while improving the observability of distribution systems. The proposed two-stage TFT-based synchrophasor estimation algorithm not only meets the P class PMU performance requirements defined in the IEC/IEEE Standard 60255-118-1:2018, but it is also fast and accurate enough to support both DER synchronous interconnection and prompt DER tripping, in compliance with the requirements of the IEEE Standard 1547-2018. Extensive simulation results in various scenarios and in noisy conditions, confirm that the proposed algorithm is capable of simultaneously fulfilling the dual role of measurement device for distribution system state estimation and synchronization module for power electronic converters. However, further studies are needed to find the best trade-off between performance and computational burden.

REFERENCES

[1] E. B. Alzate, M. Bueno-López, J. Xie, and K. Strunz, "Distribution system state estimation to support coordinated voltage-control strategies by using smart meters," *IEEE Transactions on Power Systems*, vol. 34, no. 6, pp. 5198–5207, 2019.

[2] A. Bashian, D. Macii, D. Fontanelli, and D. Petri, "A Tuned Whitening-Based Taylor-Kalman Filter for P Class Phasor Measurement Units," *IEEE Transactions on Instrumentation and Measurement*, vol. 71, pp. 1–13, 2022.

[3] S. Bu, L. G. Meegahapola, D. P. Wadduwage, and A. M. Foley, "Stability and dynamics of active distribution networks (adns) with d-pmu technology: A review," *IEEE Transactions on Power Systems*, vol. 38, no. 3, pp. 2791–2804, 2023.

[4] M. Secchi, G. Barchi, D. Macii, and D. Petri, "Smart electric vehicles charging with centralised vehicle-to-grid capability for net-load variance minimisation under increasing ev and pv penetration levels," *Sustainable Energy, Grids and Networks*, vol. 35, p. 101120, 2023.

[5] G. Barone, A. Buonomano, C. Forzano, A. Palombo, and G. Russo, "The role of energy communities in electricity grid balancing: A flexible tool for smart grid power distribution optimization," *Renewable and Sustainable Energy Reviews*, vol. 187, p. 113742, 2023.

[6] M. Secchi, G. Barchi, D. Macii, D. Moser, and D. Petri, "Multi-objective battery sizing optimisation for renewable energy communities with distribution-level constraints: A prosumer-driven perspective," *Applied Energy*, vol. 297, p. 117171, 2021.

[7] C. Muscas, M. Pau, P. A. Pegoraro, and S. Sulis, "Effects of measurements and pseudomeasurements correlation in distribution system state estimation," *IEEE Transactions on Instrumentation and Measurement*, vol. 63, no. 12, pp. 2813–2823, 2014.

[8] D. Della Giustina, M. Pau, P. A. Pegoraro, F. Ponci, and S. Sulis, "Electrical distribution system state estimation: measurement issues and challenges," *IEEE Instrumentation & Measurement Magazine*, vol. 17, no. 6, pp. 36–42, 2014.

[9] N. M. Manousakis, G. N. Korres, and P. S. Georgilakis, "Taxonomy of PMU placement methodologies," *IEEE Transactions on Power Systems*, vol. 27, no. 2, pp. 1070–1077, 2012.

[10] P. A. Pegoraro, A. Meloni, L. Atzori, P. Castello, and S. Sulis, "PMU-based distribution system state estimation with adaptive accuracy exploiting local decision metrics and IoT paradigm," *IEEE Transactions on Instrumentation and Measurement*, vol. 66, no. 4, pp. 704–714, 2017.

[11] S. Kumar, B. Tyagi, V. Kumar, and S. Chohan, "Optimization of phasor measurement units placement under contingency using reliability of network components," *IEEE Transactions on Instrumentation and Measurement*, vol. 69, no. 12, pp. 9893–9906, 2020.

[12] R. Andreoni, D. Macii, M. Brunelli, and D. Petri, "Tri-objective optimal pmu placement including accurate state estimation: The case of distribution systems," *IEEE Access*, vol. 9, pp. 62 102–62 117, 2021.

[13] A. Alimardani, F. Therrien, D. Atanackovic, J. Jatskevich, and E. Vaahedi, "Distribution system state estimation based on nonsynchronized smart meters," *IEEE Transactions on Smart Grid*, vol. 6, no. 6, pp. 2919–2928, 2015.

[14] M. Pau, E. Patti, L. Barbierato, A. Estebsari, E. Pons, F. Ponci, and A. Monti, "Design and accuracy analysis of multilevel state estimation based on smart metering infrastructure," *IEEE Transactions on Instrumentation and Measurement*, vol. 68, no. 11, pp. 4300–4312, 2019.

[15] M. R. Ahmed, J. M. Cano, P. Arboleya, L. S. Ramón, and A. Y. Abdelaziz, "DSSE in European-Type Networks Using PLC-Based Advanced Metering Infrastructure," *IEEE Transactions on Power Systems*, vol. 37, no. 5, pp. 3875–3888, 2022.

[16] G. Barchi and D. Macii, "Robust Distribution System State Estimation Based on Smart Meter Data Under High PV Penetration," in *2024 International Conference on Smart Energy Systems and Technologies (SEST)*, 2024, pp. 1–6.
[17] G. Cavraro, J. Comden, E. Dall'Anese, and A. Bernstein, "Real-time distribution system state estimation with asynchronous measurements," *IEEE Transactions on Smart Grid*, vol. 13, no. 5, pp. 3813–3822, 2022.
[18] S. Song, H. Xiong, Y. Lin, M. Huang, Z. Wei, and Z. Fang, "Robust three-phase state estimation for pv-integrated unbalanced distribution systems," *Applied Energy*, vol. 322, p. 119427, 2022.
[19] F. Messina, P. Marchi, L. Rey Vega, C. G. Galarza, and H. Laiz, "A Novel Modular Positive-Sequence Synchrophasor Estimation Algorithm for PMUs," *IEEE Transactions on Instrumentation and Measurement*, vol. 66, no. 6, pp. 1164–1175, 2017.
[20] V. N. Giotopoulos and G. N. Korres, "A Laboratory PMU Based on Third-Order Generalized Integrator Phase-Locked Loop," *IEEE Transactions on Instrumentation and Measurement*, vol. 73, pp. 1–11, 2024.
[21] D. Fontanelli and D. Macii, "Accurate time synchronization in PTP-based industrial networks with long linear paths," in *ISPCS 2010 - 2010 International IEEE Symposium on Precision Clock Synchronization for Measurement, Control and Communication, Proceedings*, 2010, p. 97 – 102.
[22] IEEE Std C37.238-2017, "IEEE standard profile for use of IEEE 1588 precision time protocol in power system applications," pp. 1–42, 2017.
[23] J. Benzaquen, M. Miranbeigi, P. Kandula, and D. Divan, "Collaborative autonomous grid-connected inverters: Flexible grid-forming inverter control for the future grid," *IEEE Electrification Magazine*, vol. 10, no. 1, pp. 22–29, 2022.
[24] R. Nicolosi, L. Piegari, and A. Benigni, "A smart PV inverter controller with PMU capability," in *2016 Clemson University Power Systems Conference (PSC)*, 2016, pp. 1–7.
[25] P. Tosato, D. Macii, M. Luiso, D. Brunelli, D. Gallo, and C. Landi, "A tuned lightweight estimation algorithm for low-cost phasor measurement units," *IEEE Transactions on Instrumentation and Measurement*, vol. 67, no. 5, pp. 1047–1057, 2018.
[26] A. Singh, K. Al Jaafari, S. K. Parida, A. Al-Durra, H. H. Zeineldin, and E. F. El-Saadany, "Dynamic synchrophasor estimation algorithm using taylor weighted least square method with harmonic input model," *IEEE Transactions on Industry Applications*, vol. 59, no. 6, pp. 7417–7427, 2023.
[27] IEC/IEEE 60255-118-1:2018, "IEEE/IEC international standard - measuring relays and protection equipment - part 118-1: Synchrophasor for power systems - measurements," pp. 1–78, 2018.
[28] IEEE Std 1547-2018 (Revision of IEEE Std 1547-2003), "IEEE standard for interconnection and interoperability of distributed energy resources with associated electric power systems interfaces," pp. 1–138, 2023.
[29] J. A. de la O Serna, "Dynamic phasor estimates for power system oscillations," *IEEE Transactions on Instrumentation and Measurement*, vol. 56, no. 5, pp. 1648–1657, 2007.
[30] M. A. Platas-Garza and J. A. de la O Serna, "Dynamic Harmonic Analysis Through Taylor–Fourier Transform," *IEEE Transactions on Instrumentation and Measurement*, vol. 60, no. 3, pp. 804–813, 2011.
[31] M. Radulović, Ž. Zečević, and B. Krstajić, "Dynamic phasor estimation by symmetric taylor weighted least square filter," *IEEE Transactions on Power Delivery*, vol. 35, no. 2, pp. 828–836, April 2020.